Nanoscale Horizons

Circular RNA oligonucleotides: Enzymatic synthesis and scaffolding for nanoconstruction

Journal:	*Nanoscale Horizons*
Manuscript ID	NH-COM-05-2024-000236.R1
Article Type:	Communication
Date Submitted by the Author:	28-Jun-2024
Complete List of Authors:	Li, Shijie; Nanjing University, School of Chemistry and Chemical Engineering Chu, Yanxin ; Nanjing University, School of Chemistry and Chemical Engineering Guo, Xin; Bruker (Beijing) Scientific Technology Co. Ltd, China Mao, Chengde; University of Purdue, Department of Chemistry Xiao, Shou-Jun; Nanjing University, School of Chemistry and Chemical Engineering

New concepts

Small-sized noncoding RNAs, including double-stranded small interfering RNAs (siRNAs) and single-stranded 20−24 nt microRNAs (miRNAs), are receiving much more attention because of the current standard-of-care linear messenger RNAs for coronavirus infections, which indicates their great therapeutic and huge market potentials. However, the natural, short, and linear RNAs are sensitive to exonuclease degradation, which is a key delivery issue for RNA pharmaceutical applications currently. One potential solution is to convert the linear RNAs into circular RNAs (circRNAs) and/or fold RNAs into nanostructures because these products are more resistant to exonuclease degradation than their cognate linear ones. Herein, we report the efficient synthesis of monomeric circRNAs in the size range of 16−44 nt with a novel DNA dumbbell splinting strategy in the T4 DNA ligation system. Such a DNA dumbbell splinting strategy was developed in Mao group (one among ours) recently for near-quantitative conversion of short linear DNAs into monomeric circular DNAs via T4 DNA ligation. In the past, in-vitro cyclisation of the short linear single-stranded RNAs via linear splinting plus enzymatic ligation often generated byproducts of concatemers rather than the monomeric circRNAs because oligomerisation releases the higher strain which should be resulted by monomerisation. Furthermore, using the synthesized 44 nt circRNA as scaffold strands, we constructed hybrid RNA:DNA and pure RNA:RNA double crossover tiles and their assemblies of nucleic acid nanotubes and flat arrays. We believe that the dumbbell splinting strategy will be highly efficient and user friendly for synthesis of both monomeric DNA and RNA oligonucleotide rings. The convenient and relatively larger scale production of circular DNA and RNA oligonucleotide molecules will expedite their application researches in depth and breadth.

COMMUNICATION

Circular RNA oligonucleotides: Enzymatic synthesis and scaffolding for nanoconstruction

Received 00th January 20xx,
Accepted 00th January 20xx

DOI: 10.1039/x0xx00000x

Shijie Li,[a] Yanxin Chu,[a] Xin Guo[b], Chengde Mao,[c,*] Shou-Jun Xiao[a,*]

We report the efficient synthesis of monomeric circular RNAs (circRNAs) in the size range of 16–44 nt with a novel DNA dumbbell splinting plus T4 DNA ligation strategy. Such a DNA dumbbell splinting strategy was developed by one group among ours recently for near-quantitative conversion of short linear DNAs into monomeric circular ones. Furthermore, using the 44 nt circRNA as scaffold strands, we constructed hybrid RNA:DNA and pure RNA:RNA double crossover tiles and their assemblies of nucleic acid nanotubes and flat arrays.

Introduction

Small-sized noncoding RNAs, including double-stranded (ds) small interfering RNAs (siRNAs) and single-stranded (ss) 20–24 nt microRNAs (miRNAs), are receiving much more attention because of the current standard-of-care linear messenger RNAs for coronavirus infections, which indicates the great therapeutic and huge market potentials.[1-4] However, the natural, short, and linear RNAs are sensitive to exonuclease degradation, which is a key delivery issue for RNA pharmaceutical applications currently. One potential solution is to convert the linear ssRNAs into circular RNAs (circRNAs) and/or fold RNAs into nanostructures because these products are more resistant to exonuclease degradation than their cognate linear ones.[5, 6] Herein, we report the preparation of small circRNAs using a novel DNA dumbbell splint plus T4 DNA ligation approach, which was invented by Mao group, one among ours, recently to convert short linear DNAs (16–40 nt) into monomeric circular DNAs in near-quantitative yields and large-scale.[7] Furthermore, we adapted three RNA folding approaches to construct hybrid RNA:DNA and pure RNA:RNA nanostructures using the core motif of double crossover (DX) tiles.

In-vitro cyclisation of short linear ssRNAs (tens of nucleotides long) often applies chemical and enzymatic ligations. In the past, all approaches exhibited drawbacks such as low yields, the higher potential of oligomerisation rather than monomerisation for ligation,[8, 9] and the byproducts formation of non-physiological linkages such as 2′-5′ phosphodiester bonds especially via chemical ligation.[8, 10] When the targeting RNA or DNA monomer ring evolves to a much smaller size less than 40 nt, the monomeric looping should generate a higher bending strain, this is why oligomerisation becomes severe for these small-sized DNA and RNA molecules because intermolecular splinting releases the higher bending strain. To overcome the competition of oligomerisation via intermolecular ligation, a novel DNA dumbbell splinting approach has been reported to be successful recently by Mao group. In this approach, they genuinely designed a dumbbell splint structure and realised near-quantitative synthesis of monomeric circular DNAs from their cognate, short, linear ssDNAs between 16–40 nt at the concentration range of 1–100 μM through the most convenient T4 DNA ligation. They explained that the two terminal hairpin loops should result in a much higher coulombic repulsion force if intermolecular oligomerisation occurred, in which is why formation of a much more stable monomer loop rather than linear or circular oligomers is preferred.[7]

Inspired by this innovation, we applied the dumbbell splinting strategy successfully in synthesis of three short circRNAs (16, 22, and 44 nt) with high efficiency via T4 DNA ligation.

Triggered by DNA nanotechnology,[11-15] RNA nanotechnology has also been developed over 30 years, mainly based on construction of rigid motifs plus connection via regular sticky end and specific kissing-loop (KL) base pairings.[16-32] For example, via the regular sticky end cohesion, Mao group constructed hybrid RNA:DNA DAE (double crossovers made of antiparallel duplexes with an even

[a] *School of Chemistry and Chemical Engineering, Nanjing University, Nanjing 210023, Jiangsu, China.*
[b] *Bruker (Beijing) Scientific Technology Co. Ltd, China*
[c] *Department of Chemistry, Purdue University, West Lafayette, Indiana 47907, USA.*
** E-mails of corresponding authors: mao@purdue.edu, sjxiao@nju.edu.cn.*
Electronic Supplementary Information (ESI) available: Materials and experimental methods, additional dPAGE photos, additional AFM images and necessary sectional profiling data, nucleic acid sequences. See DOI: 10.1039/x0xx00000x

number of half-turns distance), three-point-star, and four-point-star tiles and their corresponding 2D planar O-tiling arrays and curved E-tiling discrete polyhedra (E-tiling and O-tiling mean the inter-tile connection with a distance at an even and an odd number of half turns, respectively).[33] Franco group constructed pure RNA:RNA nanotubes via the DAE-E assembly (-E means E-tiling).[34] Andersen group transcribed long ssRNAs for self-association to form one-strand DX tiles with peripheral kissing-loops for specific base pairing, resulting in larger patches of 2D RNA arrays.[35] Xiao group, one among ours, used small circular DNAs as scaffolds to construct 1–3D DNA nanostructures.[36-39] However, as we know until now, using the small circular RNAs as scaffolds to construct 1–3D hybrid and pure RNA nanostructures have not yet been reported. Therefore, we further used the 44 nt circRNA to construct hybrid RNA:DNA and pure RNA:RNA DX tiles and nanostructures.

Results and discussion

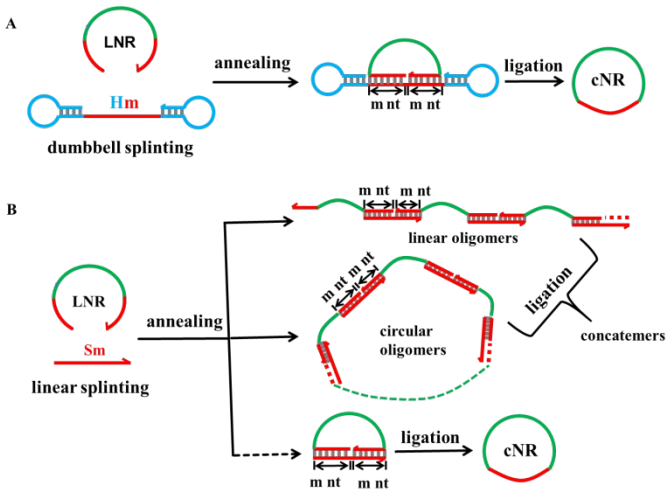

Fig. 1. Dumbbell and linear splinting strategies for cyclisation of short linear ssRNAs at the size range of 16–44 nt. (A) In the dumbbell splinting strategy, a LNR (linear N nt RNA) associates with Hm via annealing and ligates via T4 DNA ligase to form the monomeric cNR (circular N nt RNA), where the dumbbell splint Hm carries two terminal hairpin loops and a stem bearing a 2m nt ssDNA segment pairing with the LNR's 5′ and 3′ ends each by m nt. (B) In the conventional linear splinting strategy, a LNR associates with a linear Sm and ligates via T4 DNA ligase to form dominant concatemers and minor monomeric cNR molecules, where the linear splint Sm is 2m nt long and pairs with the LNR's 5′ and 3′ ends each by m nt.

Synthesis of circRNAs. The monomeric cyclisation and oligomerisation of a linear ssRNA via T4 DNA ligation are shown with their corresponding schematic approaches in Fig. 1. The T4 DNA ligation requires a splint strand to pair precisely with both 3′ and 5′ ends each by at least 6 nt long[40] because the ligase binds a little longer duplex than one helical turn (≥12 bps) for proper working.[41] The dumbbell splinting strategy (A) has much higher monomeric cyclisation efficiency due to the stronger coulombic repulsion force between the terminal hairpin loops when the sticky end cohesion occurs through intermolecular splinting as shown in (B), whereas oligomerisation occurs dominantly in the conventional linear splinting strategy (B) because it generates less free energy than monomeric cyclisation does. It is obvious that the shorter the linear ssRNAs, the stronger the bending strain generated during the monomeric cyclisation process. According to the DNA cyclisation procedure, we examined the following parameters for monomeric cyclisation of RNA, the ssRNA size and concentration, Hm with m at 4, 5, 6 nt for dumbbell splinting and Sm with m at 6 and 10 nt as controls for linear splinting, the hairpin's nT (T represents thymine) loop size in Hm with n at 1, 4, and 8, and combination of them.

Similar to the linear DNA size range chosen for the dumbbell splinting strategy, we selected three appropriate, short, linear ssRNAs at lengths of 16, 22, and 44 nt (abbreviated as L16R, L22R, and L44R molecules, respectively) as examples to examine the cyclisation efficiency. We first demonstrate the cyclisation results of miR-16, which is a natural 22 nt miRNA (L22R) and acts as a tumour suppressor in the development of diverse malignancies including breast cancer, lung cancer, cervical cancer and so on.[42] The ATP-dependent T4 DNA ligase usually catalyses the joining of nicks located in dsDNA substrates with the help of Mg^{2+}.[8, 10] Therefore, it is necessary to explore the appropriate concentrations of enzyme (Fig. S1), ATP (Fig. S2), Mg^{2+} (Fig. S3), and even the reaction temperature and time (Fig. S4) for monomeric cyclisation of short linear ssRNAs because the nick locates at the hybrid RNA:DNA substrate. Based on the above orthogonal screening experiments (Section S2 of the ESI†), the standard ligation conditions were determined and used for our RNA cyclisation reactions, unless otherwise noted. 1) The 5'-monophosphated ssRNA concentration is 10 μM, 2) the ligation is carried out with a T4 DNA ligase concentration of 2500 U/nmol RNA at 16 °C for 16 h.

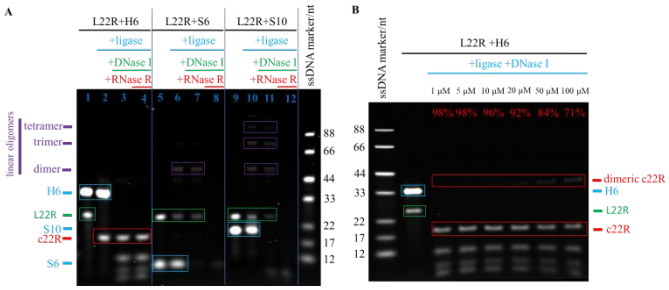

Fig. 2. (A) Enzymatic T4 DNA ligation results of L22R mediated by different splint strands (H6, S6, and S10) via the denaturing polyacrylamide gel electrophoresis (dPAGE) assay. (B) Effect of RNA (L22R) concentrations on monomeric cyclisation in H6 mediated ligation reactions. The c22R yield is indicated at the top of the gel for each corresponding concentration, and we kept the same loading molar quantity of the L22R substrate in each lane.

The L22R cyclisation results were analysed through denaturing polyacrylamide gel electrophoresis (dPAGE) (Fig. 2). We tried H6, S6, and S10 splints for ligation, separately. To clearly demonstrate the cyclisation efficiency, we generally analysed four solution samples from a series of consecutive reactions in the same ligation pot, the LNR and DNA splint mixture after mixing for blank control, after T4 DNA ligation, after DNase I digestion, and after RNase R digestion. As shown in the L22R and H6 ligation system of Fig. 2A, a strong H6 band and a medium L22R band as the blank control

evolved with carrying on the enzymatic relay reactions in series. After T4 DNA ligation, the L22R band disappeared completely and a new band moving faster than L22R occurred. After consecutive DNase I and RNase R digestions of all linear DNA and RNA residues, respectively, the H6 band disappeared in the first case, and the left band traces exhibited as the same in both cases. Because the new band remained intact, meaning that it corresponds to our target circRNA (c22R), which is resistant to both DNase I and RNase R digestions. Additional fast-moving traces below the c22R band after DNase I and RNase R digestions could be assigned to the broken pieces of DNA hairpin residues or enzyme/DNA hairpin complexes.

To compare the cyclisation results of the dumbbell splint H6 with the linear splints S6 and S10, we provided S6 and S10 mediated splinting and ligation results in Fig. 2A. The L22R band was weakened in both S6 and S10 mediated ligation reactions to some degree, instead of the c22R band, new linear oligomer bands moving more slowly than L22R appeared, which were suggested as the linear dimer, trimer, and tetramer of L22R. More slow-moving oligomer bands appeared in S10 than in S6 mediated ligations demonstrated that the S10 splinting has stronger base pairing strength for oligomerisation. After the RNase R digestion, all RNA oligomer bands disappeared, illustrating that they are linear but not circular oligomers derived from L22R.

Further, we also examined the monomeric cyclisation efficiency by changing the nT loop size in H6 from 4T to 1T and 8T. Both monomeric c22R and dimeric c22R bands appeared. With the loop size at 8T, the ratio of monomeric c22R against dimeric c22R was estimated at 6 (86/14); however, with the loop size at 1T, the ratio was estimated at 0.8 (44/56). The above results indicated that the loop sizes at 4–8T are appropriate for highly efficient monomeric cyclisation of short linear RNAs (Fig. S5).

To promote monomeric cyclisation and prevent oligomerisation of single-stranded nucleic acids in conventional linear splinting and ligation reactions, much low concentrations of the nucleic acid substrate, such as 0.1 μM, are generally used.[8, 10] However, such low concentrations decrease the enzymatic ligation efficiency tremendously and the reaction system is not suitable for large-scale production. We previously succeeded in converting the short linear ssDNAs to circular ones with very high yields in quite a wide concentration range from 1 to 100 μM,[7] so we also examined the monomeric cyclisation efficiencies of converting L22R to c22R with the L22R concentrations changing from 1, to 5, 10, 20, 50, and 100 μM, accordingly (Fig. 2B). The dPAGE results illustrated that L22R almost changed to c22R quantitatively in the concentration range of 1–10 μM; but with increasing the L22R concentrations to 20, 50, and 100 μM, the c22R yields slowly decreased to 92%, 84% and 71%, respectively; simultaneously, we also observed the increasing evolution of minor oligomer byproducts, especially the dimeric c22R. Overall, the relatively large-scale production of circRNAs from synthetic 5'-monophosphorylated ssRNA oligonucleotides is realisable.

Because the shortest linear DNA for near-quantitative cyclisation examined is 16 nt long,[7] we also examined both short linear RNAs of L16R and L14R here. Although the T4 DNA ligase normally ligates a nick when it braces a 12 bp or an even longer duplex segment, however, monomeric cyclisation of the short nucleic acids such as L16R and L14R should require even shorter effective binding domains. Thereby, except the normal H6, we also tested H5 and H4 as splint strands for cyclisation of L22R, L16R, and L14R, accordingly. The dPAGE results demonstrated that H5 converted L22R partially to c22R with a yield of 56%, but H4 failed (Fig. S6). For L16R, H6 converted L16R to both monomeric c16R with a yield of 22% and dimeric c16R with a yield of 78%, H5 converted L16R partially to c16R with a yield of 38%, but H4 failed to convert L16R to c16R or any other oligomers (Fig. S7). For L14R, H6 converted L14R only to dimeric c14R with a yield of 82% but not monomeric c14R, neither H5 nor H4 converted L14R to any monomeric c14R or other oligomers (Fig. S8). The above circular monomer and dimer yields for each LNR (N = 22, 16, 14 nt) were plotted in a histogram against H6, H5, and H4, along with their LNR-ligation dPAGE photo together, accordingly (Fig. S6–8). Still, the unpredictable cyclisation results of much short RNA oligonucleotides less than 22 nt need to be explained through further investigations of the dumbbell splinting mechanisms for cyclisation.

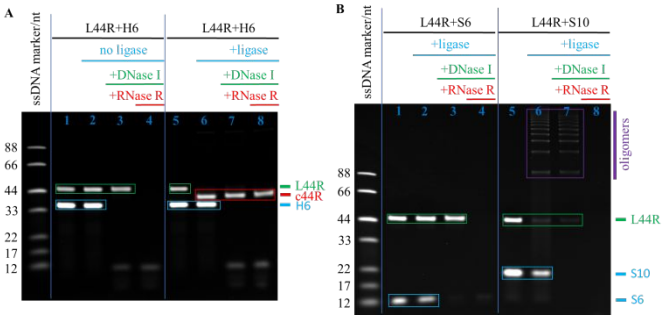

Fig. 3. Enzymatic ligations of L44R mediated by different splint strands (H6, S6 and S10) via the dPAGE assay. (A) Control and experimental groups of L44R and H6 without and with T4 DNA ligase. (B) Ligation of L44R via S6 and S10 splinting.

The dsRNA displays the A-form structure, so its periodic length is 11 bp per turn. For construction of a DAE tile, a circular ssRNA of c44R is needed to act as the scaffold. That is why we adapted a 44 nt ssRNA sequence from a literature[34] and cyclised it with the H6 splinting strategy. As shown in the left half panel of the control dPAGE photo of Fig. 3A, both L44R and H6 bands appeared clearly without addition of T4 DNA ligase; with sequential additions of DNase I and RNase R, the DNA H6 and RNA L44R bands disappeared accordingly. In the right half panel of Fig. 3A, after addition of T4 DNA ligase, L44R converted to c44R in a near-quantitative yield, and c44R remained intact after 30 min RNase R digestion at 37 ℃. Similar to the c22R experiments, we executed additional control ligation experiments with S6 and S10 as splints, separately. As shown in Fig. 3B, L44R remained nearly intact in the S6 group after both T4 DNA ligation and DNase I digestion, but disappeared after RNase R digestion; in the S10 group, most of L44R changed to linear

oligomers, which displayed a series of ladder bands above L44R after T4 DNA ligation and DNase I digestion, but disappeared after RNase R digestion. From both S6 and S10 mediated ligation results, L22R and L44R cannot be transformed to the target products c22R and c44R, respectively, meaning that the short linear splinting prefers to form linear RNA concatemers rather than monomeric cNR molecules.

Assembly of hybrid RNA:DNA and pure RNA:RNA nanostructures. We have reported the use of small circular DNAs serving as scaffold strands to construct 1–3D DNA nanostructures.[36-39] Herein, we report the use of the small circular RNA molecule, c44R, serving as scaffold strands to assemble hybrid RNA:DNA and pure RNA:RNA nanostructures via DAE-$E_{p/q}$ and DAE-$O_{p/q}$ designs, where subscripts p and q represent the numbers of inter-tile base pairs and sticky end nucleotides, respectively. Perturbations of p and q around their optimum values (generally for pure RNA:RNA nanostructures, the optimum p is 22 bp for E-tiling and 27 bp for O-tiling, and q is 5 nt for E-tiling and 6 nt for O-tiling) will screen the optimum inter-tile distance and sticky end cohesion strength for assembling perfect 2D arrays. It is accepted that a tile has both distinctively right- and left-handed faces and generally possesses an intrinsic curvature.[38] E-tiling requires that all tiles must orient with the same left- or right-handed faces toward one direction, resulting in accumulation of individual tile curvatures and formation of homogeneous nanotubes; whereas O-tiling alternates the adjacently cohered tiles between left- and right-handed faces, cancels out completely or partly the overall curvature, thus producing planar arrays and/or nonhomogenous nanotubes.[43] A DAE tile is normally composed of five short oligonucleotides, an oblang-looped scaffold strand (22 × 2 nt long for A-form nucleic acids), two main helper strands, and two auxilary helper strands (Section S4 of the ESI†). Using a transcribed, linear RNA strand serving as the scaffold, Mao group first reported the successful assembly of hybrid DAE-$O_{p/q}$ (all helper strands are short linear DNA oligonucleotides, p/q at 29/5) 2D ribbons;[33] mimicking the DNA DX assembling strategies, Franco group reported pure RNA:RNA DAE-$E_{p/q}$ assemblies, mainly composed of RNA nanotubes (monolayered rectilinear strips with p/q at 22/6, nanotubes with p/q at 23/7 and 24/8, and nanofibers with p/q at 25/9 and 26/10).[34] Andersen group reported the cotranscriptional ssRNA DX-KL origami nanotechnology to assemble pure RNA 2D nanogrids. The intertile KL interactions with a 120° arrangement result in hexagonal nanogrids.[35]

Using the circularised c44R to replace the transcriptional linear RNA molecule and serve as the scaffold strand, we constructed hybrid RNA:DNA and pure RNA:RNA DAE tiles; further applying the simple one-tile assembly strategy, we constructed hybrid DAE-$E_{p/q}$ nanotubes and DAE-$O_{p/q}$ nanogrids, pure DAE-$E_{p/q}$ nanotubes via the sticky end cohesion, and DAE-KL honeycomb-like nanogrids via the kissing-loop interaction.

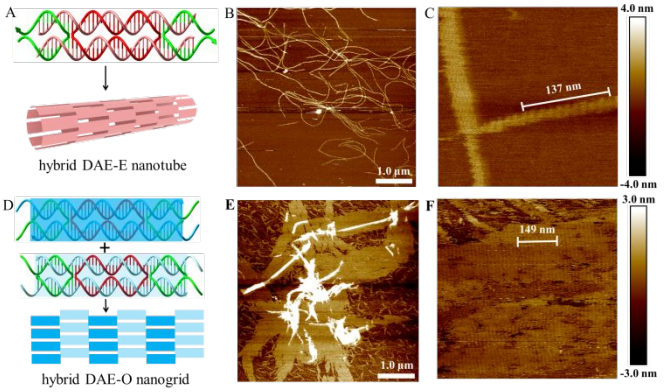

Fig. 4. Self-assembly of hybrid c44R:DNA nanostructures via DAE-E and DAE-O strategies. (A) Schematic diagram showing a DAE tile and the assembly of a nanotube via DAE-E. (B, C) Zoomed-out and zoomed-in AFM images of DAE-$E_{21/5}$ nanotubes. (D) Schematic diagram showing a DAE tile with two distinctive faces (blue and light blue) and the assembly of a nanogrid via DAE-O. (E, F) Zoomed-out and zoomed-in AFM images of DAE-$O_{27/5}$ nanogrids.

The hybrid DAE-$E_{21/5}$ and DAE-$O_{27/5}$ designs and their nanostructures are shown in Fig. 4. Following the general E- and O-tiling rules in DNA nanotechnology, the hybrid DAE-$E_{21/5}$ provided high-yield mature nanotubes with a diameter at ~30 nm and lengths ranged between 4 and 9 μm (Fig. 4B, S9). In the zoomed-in AFM image (Fig. 4C), the periodic distance of a single tile length was measured at 13.7 nm (137 nm/10), which is close to the theoretical value 13.6 nm (3.4 nm/turn × 4 turns). Perturbations of p/q to 20/4 and 22/6 also generated nanotubes, which have the similar tube diameter as p/q at 21/5, but in a bit shorter lengths ranged at 2–7 μm and with relatively lower yields (Fig. S10, S11). In addition, we also imaged the hybrid DAE-$E_{21/5}$ nanotubes stored at 4 ℃ for about a month and found that they kept intact (Fig. S12), demonstrating that the hybrid RNA:DNA nanostructures are quite stable under our routine storage and processing conditions. The hybrid DAE-$O_{27/5}$ provided perfect 2D flat arrays in Fig. 4E, F and S13, where the periodic distance of 14.9 nm (149 nm/10) between stripes corresponds to a DAE-$O_{27/5}$ unit length (the theoretical value is 3.4 nm/turn × 4.5 turns = 15.3 nm). Perturbations of p/q to 26/4 gave monolayered strips with a width at ~121.0 nm and lengths ranged between 2 and 6 μm (Fig. S14), further to 28/6 and 29/5 only generated tile-oligomer fragments (Fig. S15).

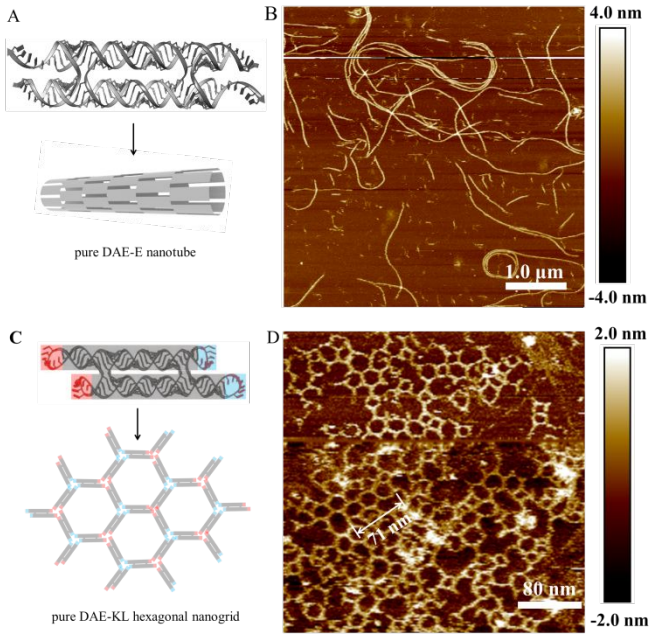

Fig. 5. Pure RNA:RNA nanostructures with c44R serving as scaffold strands via DAE-E and two-strand DAE-KL assembly strategies. (A) Schematic diagram showing a pure RNA:RNA DAE tile and the assembly of a nanotube via DAE-E. (B) AFM image of many DAE-$E_{22/6}$ nanotubes. (C) Schematic diagram showing a two-strand DAE-KL unit and the hexagonal assembly model via the 120° kissing loop interaction. (D) AFM image of two-strand DAE-KL hexagonal nanogrids.

With c44R serving as the scaffold strands, we also succeeded in assembling pure RNA:RNA DAE-$E_{p/q}$ nanotubes and DAE-KL hexagonal nanogrids (Fig. 5). We designed five DAE-$E_{p/q}$ variants with p/q perturbed at 22/4, 22/6, 23/5, 23/7, and 24/8. Among these variants, DAE-$E_{22/6}$ performed best to provide ripe, rigid RNA nanotubes with a diameter at ~39.0 nm, a height at ~3.6 nm, and lengths ranged between 2 and 7 μm (Fig. 5B, S16); DAE-$E_{22/4}$ and DAE-$E_{23/5}$ formed similar but low-yield nanotubes with relatively shorter lengths ranged between 2 and 5 μm, which were accompanied with densely distributed tile-oligomer fragments (Fig. S17, S18); finally, DAE-$E_{23/7}$ and DAE-$E_{24/8}$ only generated much shorter nanofibers with lengths ranged between 0.5 and 2 μm (Fig. S19). The above results presented the similar assembling tendency but differentiated slightly in detail with those reported in the reference using the linear RNA strand for scaffolding.[34] For example, in the reference, DAE-$E_{22/6}$ cannot form nanotubes but lengthy monolayered strips, while both DAE-$E_{23/7}$ and DAE-$E_{24/8}$ designs were optimal for assembling nanotubes, among which a few exceeded 10 μm in length. The reason for the assembling differences might be mainly attributed to the topology difference of the scaffold strands; however, the heterogeneity of the *in vitro* transcribed RNA strands, especially the considerable 3′ terminal heterogeneity, should also be accounted for.[8, 44, 45]

Inspired by the cotranscriptional, one-strand DX origami technology via kissing-loop base pairing interactions,[35] we designed a two-strand DAE-KL system for self-assembly (Fig. 5C). With the c44R as the core scaffold, a transcriptional ssRNA complements to c44R and form the DAE core domain, and the rest of the ssRNA strand self-associates at the four corners of the DAE-KL unit to generate two peripheral 120° KL pairs. The one-tile DAE-KL units assembled mainly to hexagonal nanogrids with a linear lattice constant at 23.7 nm (71 nm/3), very close to the theoretical value of 23.6 nm. Additional deformed polygons such as diamonds, pentagons, elongated hexagons, heptagons, and even octagons also occurred minorly. The above observations can be accounted for the formation of different vertex joints: regularly three-branched (statistically estimated at ~70%), and minorly occurred two-branched and four-branched (Fig. 5D, S20).

Conclusions

In summary, using the newly established dumbbell splinting plus T4 DNA ligation strategy, we successfully converted two short, linear ssRNAs, miR-16 at 22 nt and a 44 nt strand adapted from the literature[34], to their respective monomeric circRNAs in near-quantitative yields. We screened the experimental conditions, including the concentrations of four components, RNA substrate, T4 DNA ligase, ATP, and Mg^{2+}, and temperature plus incubation time for optimisation of monomeric cyclisation ligations. On this basis, we further applied the c44R strand to construct both hybrid and pure RNA DAE tiles and their DAE-$E_{p/q}$, DAE-$O_{p/q}$, and DAE-KL assemblies with perturbed p/q variants, which appear as nanotubes, flat nanoarrays, and wireframe nanogrid patterns.

Author contributions

SL, CM, and SJX developed the concept for this work through discussion (conceptualisation). SL conducted experiments and analysis including material synthesis, denaturing PAGE assay, RNA purification, nanostructure assembling and AFM imaging (investigation & formal analysis), YC and XG supported the experiments in transcription and AFM imaging, respectively (investigation). SL gathered and trimmed the data and constructed figures for visualisation and presentation (data curation and visualisation). SL and SJX wrote the original draft (writing). CM and SJX reviewed and edited the manuscript (writing and editing).

Conflicts of interest

There are no conflicts to declare.

Acknowledgements

SJX acknowledges the financial support from the National Natural Science Foundation of China (91753134 and 21571100). CM acknowledges the financial support from the NSF (2025187 and 2107393).

Notes and references

1 Y. M. Demirci and M. D. Sacar Demirci, *J. Integr. Bioinform.*, 2021, **18**, 45-50.
2 X. Liu, W. Xiong, M. Ye, T. Lu, K. Yuan, S. Chang, Y. Han, Y. Wang, L. Lu and Y. Bao, *Signal Transduct Target Ther.*, 2023, **8**, 441.
3 S. M. Nur, M. A. Hasan, M. A. Amin, M. Hossain and T. Sharmin, *Interdiscip. Sci.*, 2015, **7**, 257-265.
4 S. S. Sohrab, S. A. El-Kafrawy, Z. Mirza, M. A. Kamal and E. I. Azhar, *Curr. Pharm. Des.*, 2018, **24**, 62-77.
5 Y. Enuka, M. Lauriola, M. E. Feldman, A. Sas-Chen, I. Ulitsky and Y. Yarden, *Nucleic Acids Res.*, 2016, **44**, 1370-1383.
6 S. Umekage and Y. Kikuchi, *J. Biotechnol.*, 2009, **139**, 265-272.
7 V. E. Paluzzi, C. Zhang and C. Mao, *Angew. Chem. Int. Ed. Engl.*, 2023, **62**, e202218443.
8 P. Obi and Y. G. Chen, *Methods*, 2021, **196**, 85-103.
9 S. Muller and B. Appel, *RNA Biol.*, 2017, **14**, 1018-1027.
10 M. J. Moore and C. C. Query, *Methods Enzymol.*, 2000, **317**, 109-123.
11 Q. Hu, H. Li, L. Wang, H. Gu and C. Fan, *Chem. Rev.*, 2019, **119**, 6459-6506.
12 S. Nummelin, J. Kommeri, M. A. Kostiainen and V. Linko, *Adv. Mater.*, 2018, **30**, e1703721.
13 Y. He, T. Ye, M. Su, C. Zhang, A. E. Ribbe, W. Jiang and C. Mao, *Nature*, 2008, **452**, 198-201.
14 P. Yin, R. F. Hariadi, S. Sahu, H. M. Choi, S. H. Park, T. H. Labean and J. H. Reif, *Science*, 2008, **321**, 824-826.
15 P. W. Rothemund, *Nature*, 2006, **440**, 297-302.
16 D. Jasinski, F. Haque, D. W. Binzel and P. Guo, *ACS Nano.*, 2017, **11**, 1142-1164.
17 E. Poppleton, N. Urbanek, T. Chakraborty, A. Griffo, L. Monari and K. Gopfrich, *RNA Biol.*, 2023, **20**, 510-524.
18 D. Han, X. Qi, C. Myhrvold, B. Wang, M. Dai, S. Jiang, M. Bates, Y. Liu, B. An, F. Zhang, H. Yan and P. Yin, *Science*, 2017, **358**, eaao2648.
19 W. Grabow and L. Jaeger, *F1000Prime Rep.*, 2013, **5**, 46.
20 E. Westhof, B. Masquida and L. Jaeger, *Fold Des.*, 1996, **1**, R78-88.
21 W. W. Grabow and L. Jaeger, *Acc Chem Res.*, 2014, **47**, 1871-1880.
22 C. Geary, A. Chworos, E. Verzemnieks, N. R. Voss and L. Jaeger, *Nano Lett.*, 2017, **17**, 7095-7101.
23 N. B. Leontis and E. Westhof, *Science*, 2014, **345**, 732-733.
24 A. S. Abu Almakarem, A. I. Petrov, J. Stombaugh, C. L. Zirbel and N. B. Leontis, *Nucleic Acids Res.*, 2012, **40**, 1407-1423.
25 K. A. Afonin, M. Viard, A. Y. Koyfman, A. N. Martins, W. K. Kasprzak, M. Panigaj, R. Desai, A. Santhanam, W. W. Grabow, L. Jaeger, E. Heldman, J. Reiser, W. Chiu, E. O. Freed and B. A. Shapiro, *Nano Lett.*, 2014, **14**, 5662-5671.
26 G. C. Shukla, F. Haque, Y. Tor, L. M. Wilhelmsson, J. J. Toulme, H. Isambert, P. Guo, J. J. Rossi, S. A. Tenenbaum and B. A. Shapiro, *ACS Nano.*, 2011, **5**, 3405-3418.
27 K. A. Afonin, M. Viard, I. Kagiampakis, C. L. Case, M. A. Dobrovolskaia, J. Hofmann, A. Vrzak, M. Kireeva, W. K. Kasprzak, V. N. KewalRamani and B. A. Shapiro, *ACS Nano.*, 2015, **9**, 251-259.
28 L. Rolband, D. Beasock, Y. Wang, Y. G. Shu, J. D. Dinman, T. Schlick, Y. Zhou, J. S. Kieft, S. J. Chen, G. Bussi, A. Oukhaled, X. Gao, P. Sulc, D. Binzel, A. S. Bhullar, C. Liang, P. Guo and K. A. Afonin, *Comput. Struct. Biotechnol. J.*, 2022, **20**, 6120-6137.
29 M. Chandler, T. Lyalina, J. Halman, L. Rackley, L. Lee, D. Dang, W. Ke, S. Sajja, S. Woods, S. Acharya, E. Baumgarten, J. Christopher, E. Elshalia, G. Hrebien, K. Kublank, S. Saleh, B. Stallings, M. Tafere, C. Striplin and K. A. Afonin, *Molecules*, 2018, **23**.
30 J. M. Stewart, M. Viard, H. K. Subramanian, B. K. Roark, K. A. Afonin and E. Franco, *Nanoscale*, 2016, **8**, 17542-17550.
31 M. F. Parsons, M. F. Allan, S. Li, T. R. Shepherd, S. Ratanalert, K. Zhang, K. M. Pullen, W. Chiu, S. Rouskin and M. Bathe, *Nat. Commun.*, 2023, **14**, 382.
32 E. C. Wamhoff, L. Ronsard, J. Feldman, G. A. Knappe, B. M. Hauser, A. Romanov, J. B. Case, S. Sanapala, E. C. Lam, K. J. S. Denis, J. Boucau, A. K. Barczak, A. B. Balazs, M. S. Diamond, A. G. Schmidt, D. Lingwood and M. Bathe, *Nat. Commun.*, 2024, **15**, 795.
33 S. H. Ko, M. Su, C. Zhang, A. E. Ribbe, W. Jiang and C. Mao, *Nat. Chem.*, 2010, **2**, 1050-1055.
34 J. M. Stewart, C. Geary and E. Franco, *ACS Nano.*, 2019, **13**, 5214-5221.
35 C. Geary, P. W. Rothemund and E. S. Andersen, *Science*, 2014, **345**, 799-804.
36 M. Wang, H. Huang, Z. Zhang and S. J. Xiao, *Nanoscale*, 2016, **8**, 18870-18875.
37 M. Ali, N. Afshan, C. Jiang, H. Zheng and S. J. Xiao, *Nanoscale*, 2019, **11**, 22216-22221.
38 C. Jiang, B. Lu, W. Zhang, Y. P. Ohayon, F. Feng, S. Li, N. C. Seeman, S. -J. Xiao, *J. Amer. Chem. Soc.*, 2022, **144**, 6759-6769.
39 Y. Wang, W. Ge, B. Lu, J. J. Zhu and S. J. Xiao, *Nanoscale.*, 2020, **12**, 19597-19603.
40 R. An, Q. Li, Y. Fan, J. Li, X. Pan, M. Komiyama and X. Liang, *Nucleic Acids Res.*, 2017, **45**, e139.
41 K. Shi, T. E. Bohl, J. Park, A. Zasada, S. Malik, S. Banerjee, V. Tran, N. Li, Z. Yin, F. Kurniawan, K. Orellana and H. Aihara, *Nucleic Acids Res.*, 2018, **46**, 10474-10488.
42 S. Ghafouri-Fard, T. Khoshbakht, B. M. Hussen, S. T. Abdullah, M. Taheri and M. Samadian, *Cancer Cell Int.*, 2022, **22**, 342.
43 H. Yan, S. H. Park, G. Finkelstein, J. H. Reif and T. H. LaBean, *Science*, 2003, **301**, 1882-1884.
44 J. F. Milligan, D. R. Groebe, G. W. Witherell and O. C. Uhlenbeck, *Nucleic Acids Res.*, 1987, **15**, 8783-8798.
45 Y. Gholamalipour, A. Karunanayake Mudiyanselage and C. T. Martin, *Nucleic Acids Res.*, 2018, **46**, 9253-9263.

The data supporting this article have been included as part of the Supplementary Information.